Materials Science in Semiconductor Processing 75 (2018) 221–233

Contents lists available at ScienceDirect

Materials Science in Semiconductor Processing

journal homepage: www.elsevier.com/locate/mssp

Physical properties of solution processable n-type Fe and Al co-doped ZnO nanostructured thin films: Role of Al doping levels and annealing

A. Goktas[a,*], F. Aslan[a], B. Yeşilata[b], İ. Boz[a]

[a] Harran University, Faculty of Arts and Sciences, Department of Physics, Sanliurfa 63300, Turkey
[b] Harran University, Mechanical Engineering Department, Sanliurfa 63300, Turkey

ARTICLE INFO

Keywords:
Al and Fe co-doped ZnO thin films
Solution process
Annealing
Refractive index
Oxygen vacancy
Room temperature ferromagnetism
Grain boundary effect

ABSTRACT

The role of annealing temperature and Fe and Al co-doping on structural, optical, electrical and magnetic properties of solution processable ZnO thin films were investigated. ZnO:Fe thin films fixed with 2% of typical ferrous component were obtained to examine the role of 1–10% Al doping. X-ray diffraction analyses clearly indicates that the films to be polycrystalline and preferentially oriented along the c-axis of the hexagonal wurtzite structure. The film thickness, homogeneous distribution and decreasing/increasing of grain size dependence on Al content/annealing temperature (T_A) were assessed by scanning electron microscopy. X-ray photoelectron spectroscopy revealed that Al^{3+} and Fe^{2+} ions to substitute for Zn^{2+} without changing the wurtzite structure. A slight decrease in the optical band gap of ZnO at fixed Fe dopant and a considerable increase of the optical band gap with increased Al doping concentrations and T_A were observed. The refractive index increases with the fixed Fe dopant level and then decreases by Al doping levels, whereas the extinction coefficient clearly increases depended on both of Fe and Al concentrations. The refractive index and extinction coefficient both decrease with T_A. Hall measurements show n-type conductivity and the increase of charge carrier concentration by Al doping levels and T_A. Magnetic studies indicate room temperature ferromagnetism in Al and Fe co-doped ZnO thin films, whereas no room temperature ferromagnetism for the Fe-doped ZnO thin films was observed. An enhanced room temperature ferromagnetism in Al and Fe co-doped ZnO thin films was observed to depend on T_A.

1. Introduction

A great deal of effort has been devoted to transparent conductive oxide (TCO) thin films due to their tunable structural, optical and magnetic properties by inserting transition metal (TM) dopants in the last decade [1–5]. It is known that the TM can tune the physical properties of the TCO thin films because of the exchange interaction between the s and p electrons of host ZnO and d electron of TM ions [6]. Among the various TCO candidates, ZnO is the most important one due to its unique properties such as the wider direct band gap energy (3.3 eV), the larger exciton binding energy (60 meV) and the excellent physical and chemical stability. These properties make it a perfect host candidate for optoelectronic devices like solar cells, flat panel displays, gas sensors and UV semiconductor lasers [7–10].

In addition, ZnO is an attractive and promising diluted magnetic semiconductor (DMS) material since it exhibits ferromagnetism by doping transition metals such as Mn, Fe and Co at room temperature (RT) and is highly transparent to the visible light [1,11–13]. It is reported that the ferromagnetism of polycrystalline pure and doped ZnO can be caused by having enough grain boundaries [37,38]. Moreover, doping additional carriers into ZnO, such as Al, Cu and Ga elements, may also result in RT ferromagnetism [14–18]. For example, Lu et al. [14] reported an enhancement of the magnetization value of ZnCoO thin films by additional Al doping, produced by molecular beam epitaxy (MBE) technique. Similar enhancements in the magnetization values were also observed in Al doped ZnCoO and ZnMnO thin films produced by sol-gel [15] and sol-gel derived auto combustion [16] techniques, respectively. However, limited reports are available on trivalent and Fe

* Corresponding author.
E-mail address: agoktas@harran.edu.tr (A. Goktas).

https://doi.org/10.1016/j.mssp.2017.11.033
Received 2 November 2017; Received in revised form 20 November 2017; Accepted 22 November 2017
Available online 13 December 2017
1369-8001/

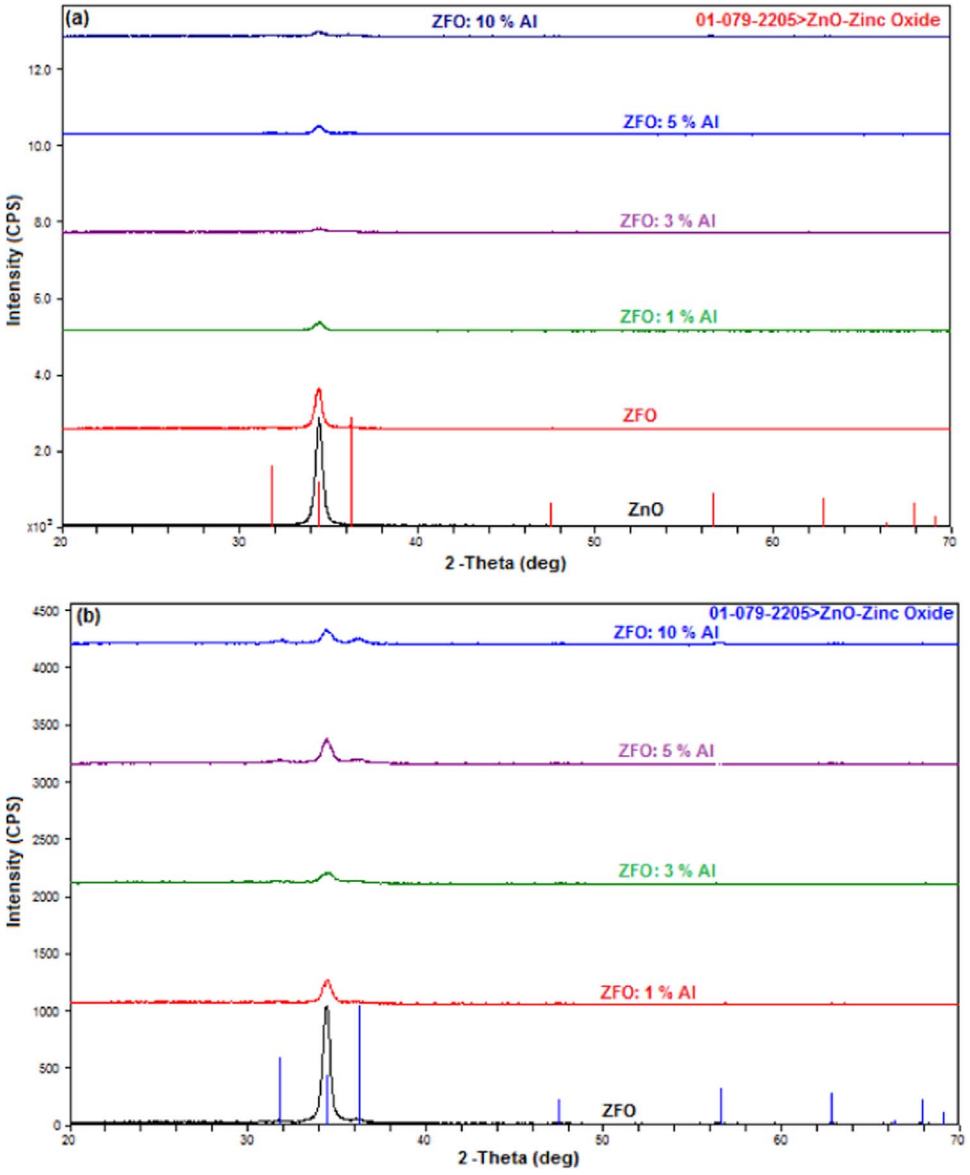

Fig. 1. (a) XRD patterns of ZnO, ZFO and ZFO: Al (1%, 3%, 5% and 10%), (b) ZFO and ZFO: Al (1%, 3%, 5% and 10%), (c) ZFO: Al (1%, 3%, 5% and 10%) thin films, (d-h) research for secondary phases in ZFO: Al (1%, 3%, 5% and 10%) thin films and (i) ZFO: Al (1%) thin films annealed at different T_A.

co-doped ZnO thin films. Recently, an incremental trend in magnetization of Al-doped ZnFeO derived via pulsed laser deposition (PLD) technique [19] and B doped ZFO produced by a modified and chemically derived citrate gel method has also been reported [20].

Inconsistent with the above mentioned studies, the lack of RT ferromagnetism in the $Zn_{1-x}Fe_xO$ and ZnCoO:Al films were observed by Goktas et al. [3] and Kaspar et al. [21], respectively. The results obtained to date suggest a clear discrepancy among findings, probably due to the differences in film growth methods, the annealing conditions and the chemicals used as starting powders type and solvents.

In the present study, the Al and Fe co-doped ZnO thin films were derived by solution and coating process, which is a comparatively simple, low cost and convenient to synthesis nanoparticles and thin films with high purity and homogeneity [1,3,5]. Such a thin film Fe and Al co-doped ZnO, produced by solution technique has not been studied yet in the literature. For this reason, this is the first report revealing the role of annealing temperature, Al and Fe co-doping contents on the structural, electrical, optical and magnetic properties of ZnO thin films synthesized by solution process.

2. Experimental details

ZnO thin films with fixed Fe doping ratio (2%) and different Al doping levels (1–10%) and average film thickness of 900 nm were deposited on glass substrates by sol-gel dip coating technique. To synthesize the films, the sols were formed by using appropriate molar

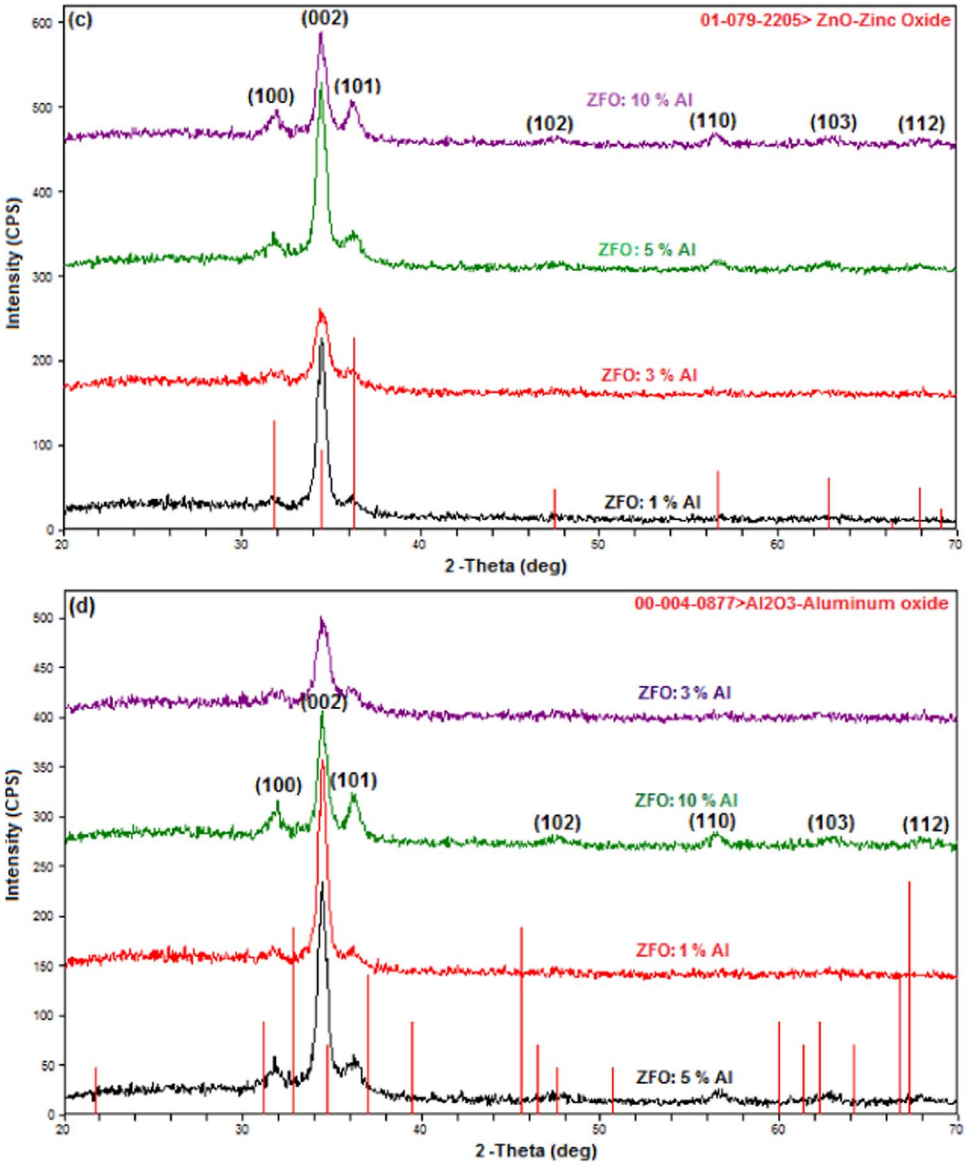

Fig. 1. (*continued*)

ratios of the zinc acetate dihydrate Zn $(CH_3COO)_2x2H_2O$ (99.99%), ferrous nitrate nonahydrate $(Fe(NO_3)_3)x9H_2O$ (99.95%), aluminum nitrate nonahydrate $(Al(NO_3)_3)x9H_2O$ (99%) powders, 2-methoxyethanol ($CH_3OCH_2CH_2OH$, solvent) and ethanolamine (stabilizer). The powders were dissolved in 20 ml of the 2-methoxyethanol under continuous stirring. The typical ferrous (Fe) content was fixed at 2%, while aluminum (Al) contents varied from 1% to 10%. Then 0.5 ml ethanolamine was added drop wise to keep the pH of the solutions between 6.5 and 7.5. The total mixture was then mixed for about 1 h to obtain clear and homogeneous solutions. Finally, the solutions were aged for 36 h before the film deposition.

The Al and Fe-doped ZnO films were deposited by dip coating technique on the glass substrates at 500 °C for 10 min. The films were annealed at 600 °C for 1 h. To investigate the role of the annealing temperature (T_A) the selected 1% Al-doped ZnO:Fe (ZFO) film was also deposited on quartz glass via the same technique at T_A of 650 and 700 °C for 1 h. To get the desired film thickness, 20 dipping times was applied for all samples to keep the film thickness precisely. In order to evaluate the crystallite phase and phase purity of the films Rigaku Ultima III (CuKα, 40 kV, 40 mA, 1.54 Å) x-ray diffraction (XRD) unit was used with scan step of 0.02°(θ) in scanning range between 20° and 70° (2θ). The valance state of the Zn, Fe and Al elements was carried out by x-ray photoelectron spectroscopy (XPS) (PHI-5000 Versaprobe) spectrometer system. The morphology of the Al-doped ZFO films was investigated by SEM (Zeiss Evo 50) system attached with Röntec 3000 detector. Optical characterizations were performed in the wavelength range of 300–900 nm by Ultraviolet–visible (Uv) spectrophotometer (Perkin Elmer 45 UV–VIS). Magnetization studies were carried out using a vibrating sample magnetometer, VSM (Cryogenic Limited PPMS, XL-5T) in the temperature range 2–350 K. Electrical transport properties including Hall measurements were carried out using a four terminal van der Pauw configuration in magnetic fields of up to 1 T.

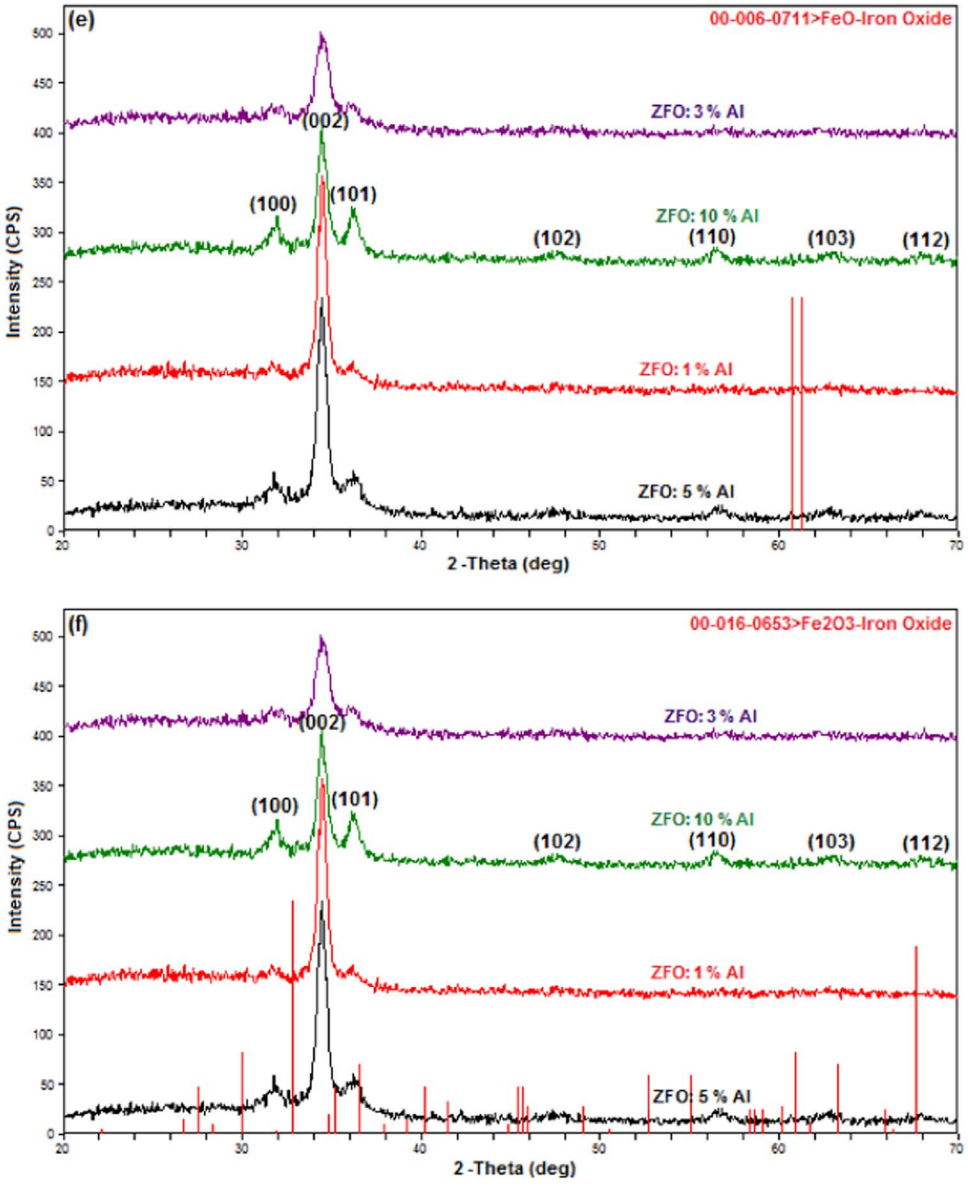

Fig. 1. (*continued*)

3. Results and discussions

3.1. Structural properties

We first present the XRD patterns of the Al-doped ZFO thin films taken at room temperature. The results are shown in Fig. 1a-i. The diffraction lines of the films are mainly matched with JCPDS card no. 01-079-2205, indicating hexagonal wurtzite type structure of ZnO having the polycrystalline nature. The preferred diffraction lines along (002) plane are observed for all films under consideration. As the Al doping level increased, the peak intensity of the (002) plane profoundly decreased except for 5% Al doping level. This is probably due to the fact that the dopants (Fe, Al) incorporation declines the crystallinity of the films due to the different ionic size of Zn, Fe and Al as observed in earlier studies [3,16,19]. The (100), (101), (102), (110), (103) and (112) planes also exist for the films, depending on the peak intensity of (002) plane as seen in Fig. 1c-h. On the other hand, no extra diffraction lines corresponding to the metallic Al/Fe or secondary and impurity phases of Al and Fe exist (Al_2O_3, FeO, γ-Fe_2O_3, Fe_3O_4 and $ZnFe_2O_4$ as seen in Fig. 1d-h) which demonstrate proper incorporation of Al^{3+} and Fe^{2+} ions into Zn^{2+} lattice site. The XRD patterns at different T_A (600, 650 and 700 °C) for the 1% Al-doped ZFO is also presented in Fig. 1i, which also confirm the same results with the other Al-doped ZFO thin films as mentioned above. It is observed that the peak intensity of (002) plane of 1% Al-doped ZFO is gradually increased as T_A changed from 600 to 700 °C.

The crystallite size (D_{hkl}) of the films is calculated by using Scherrer's equation [3]. The results are summarized in Table 1. The crystalline quality of the films is gradually declined except for the 5% Al with increased Al doping level. However, the improvement of D_{002} is

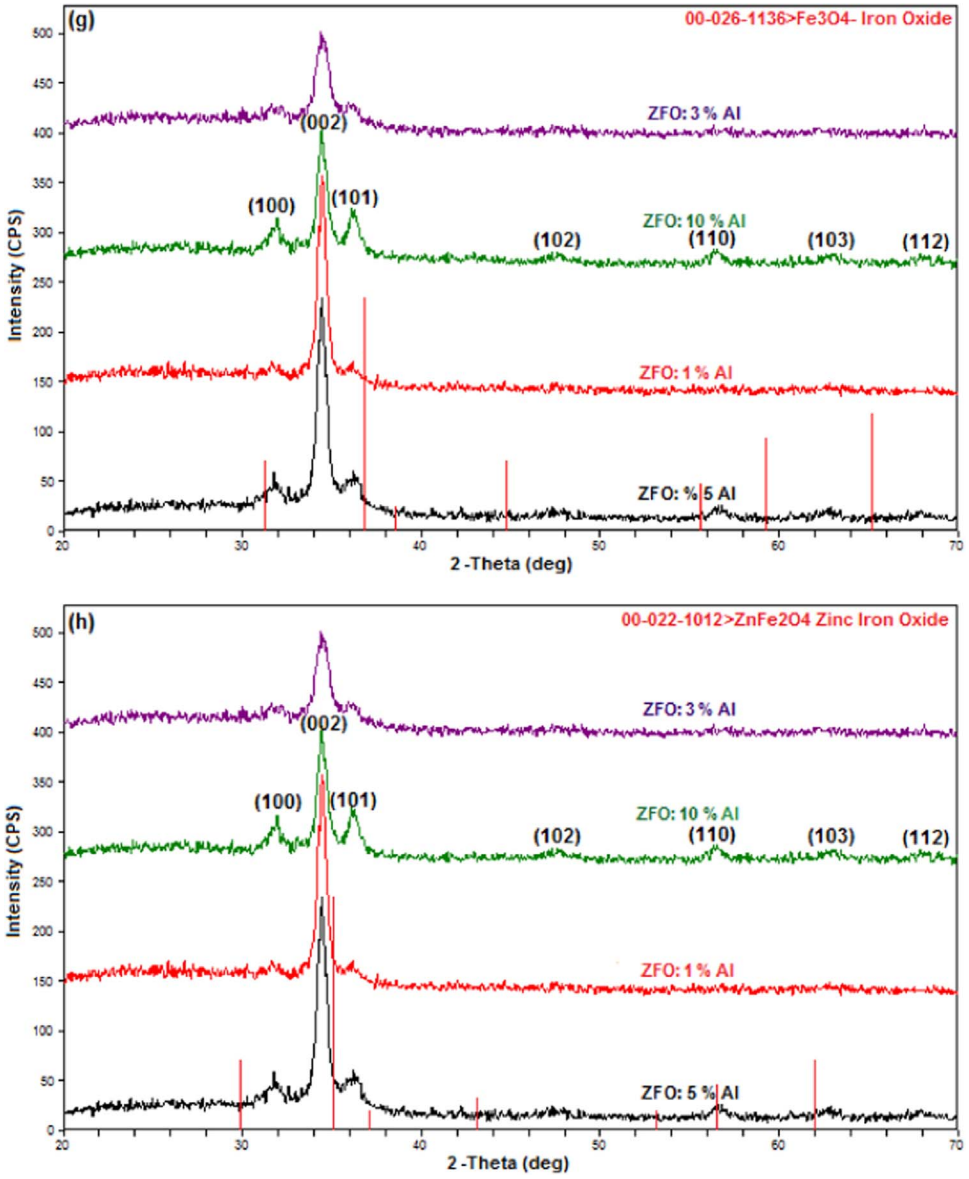

Fig. 1. (*continued*)

observed for 1% Al doped ZFO with enhanced T_A. These behaviors may possibly be attributed to the decrement/increment of the peak intensity of (002) plane and decrease/increase in the full width at half maximum (FWHM) of (002) plane. It is important to notice that the *c* lattice parameter of the thin films increases by the first inclusion of Fe dopant and then also increases by an initial doping ratio of Al, in comparison to the ZnO and ZFO, respectively. Further increase in Al doping level causes in a nonlinear decrease in the *c* lattice parameter. On the other hand, the linear increase in the *c* is founded for the samples annealed at different T_A. The irregular variations in *c* can be addressed to the combination of several factors; such as the difference between the atomic radii of dopants ($r_{Al}{}^{3+}$ = 0.54 Å and $r_{Fe}{}^{2+}$ = 0.63 Å, for tetrahedral coordination) and the host materials ($r_{Zn}{}^{2+}$ = 0.60 Å, for tetrahedral coordination), average crystal size D_{hkl}, micro strain inside the lattice, the impurities having different ionic radii in the lattice and the difference in the thermal expansion coefficients of ZnO film (7×10^{-6}/°C) glass substrates (9×10^{-6}/°C), as implied in previous studies [3,5,18].

We next present the surface images of the ZnO, ZFO, and Al-doped ZFO thin films given in Fig. 2(a-d). All the images exhibit spherically shaped grains, which are randomly distributed. Inclusion of Fe dopant and increasing of the Al doping level have the same effect on grain size of the films, resulting in a decrease. However, T_A leads to increased grain size of the 1% Al doped ZFO thin films as seen in Fig. 2(e-g). The clear indication of decreasing/increasing in crystalline quality of the films is supported by calculations of the D_{002}. The results are in well agreement with previously reported studies [15,16].

To evaluate the grain boundary effect on the physical properties of prepared thin films the average mean grain size (G_S) of them was estimated from the surface images (Fig. 2a-g). The estimated G_S values

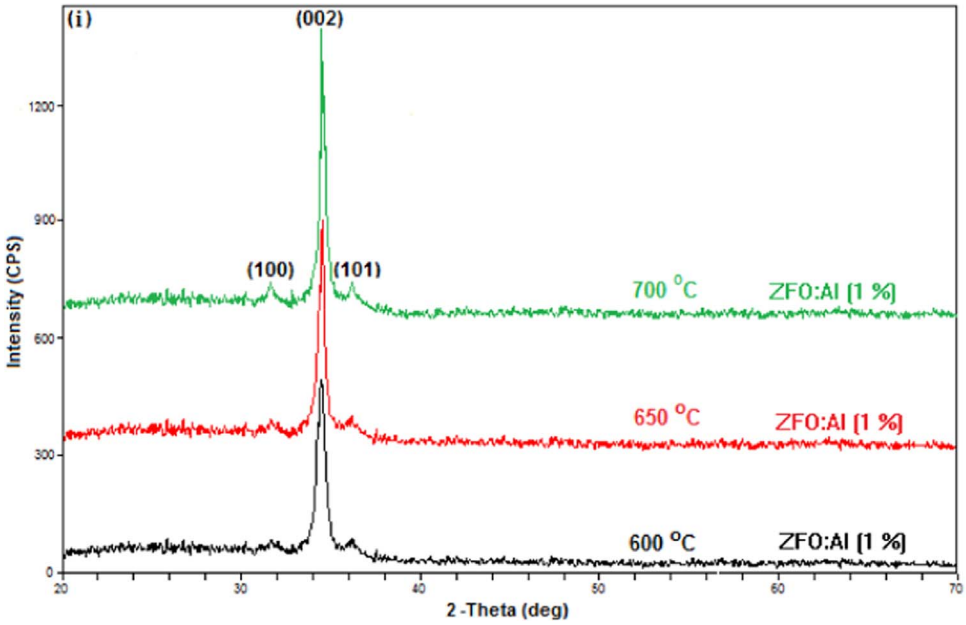

Fig. 1. (*continued*)

Table 1
Summary of the selected structural properties of ZnO, ZFO and ZFO: Al (1%, 3%, 5% and 10%) thin films depended on T_A.

Chemical composition	FWHM (β°)	2θ (deg.)	D_{002}(nm)	c (nm)	T_A (°C)
ZnO	0.36	34.46	27	5.207	600
ZFO	0.44	34.44	22	5.210	600
ZFO: Al (1%)	0.70	34.42	14	5.212	600
ZFO: Al (3%)	0.94	34.52	10	5.196	600
ZFO: Al (5%)	0.81	34.46	12	5.207	600
ZFO: Al (10%)	1.08	34.50	9	5.200	600
ZFO: Al (1%)	0.54	34.41	18	5.214	650
ZFO: Al (1%)	0.40	34.40	24	5.216	700

are approximately 35, 50, 30, 25, 35, 45 and 50 nm for the ZnO, ZFO, ZFO:Al 1%, ZFOAl %3, ZFO:Al 10%, ZFO:Al 1% (T_A = 600 °C), ZFO:Al 1% (T_A = 650 °C) and ZFO:Al 1% (T_A = 700 °C), respectively. These values are higher than those of D_{hkl} confirming fact that the grains are composed of many crystals. According to theoretical work of Straumal et al. [22] the GB-area-to-volume ratio is $sGB = 1.65/G_S$, where G_S is the mean grain size. Therefore, the *sGB* values of undoped and doped ZnO thin films are around 47.1×10^6, 33×10^6, 55×10^6, 66×10^6, 47.1×10^6, 36×10^6, and 33×10^6 m^2/m^3 for the ZnO, ZFO, ZFO:Al 1%, ZFOAl %3, ZFO:Al 10%, ZFO:Al 1% (T_A = 600 °C), ZFO:Al 1% (T_A = 650 °C) and ZFO:Al 1% (T_A = 700 °C), respectively. It is found that the *sGB* is initially decreased on Fe doping and then increased by enhanced Al doping ratio compared with undoped ZnO thin films. In addition, increased T_A results in decreased *sGB* due to the increased G_S.

We provide Fig. 3 to show that the film thickness of the samples is around 900 nm. As a supportive proof, the EDX spectrum of the films is presented in Fig. 4, confirming the presence of Zn, Fe, Al, O and Si and the increment of the Al content along with its peak intensity.

XPS studies are important to have knowledge about the valance states of the dopants and host elements. The XPS results are given in Fig. 5(a-c). The XPS spectra of ZFO: Al (3%) thin film clearly exhibits the presence of the Zn, Fe, and Al elements. The peak positions corresponding to the Zn 2p3/2 and 2p1/2 are located respectively at 1021.5 and 1044.5 eV, as seen in Fig. 5a. This is strong evidence of the Zn^{2+} since its binding energy position of Zn 2p spectra is approximately close to the standard data of ZnO [5]. The peak position of the Fe $2p_{1/2}$ and $2p_{3/2}$ are observed at a corresponding energy of 722.7 and 709.4 eV (see Fig. 5b). This finding is also well consistent with the XPS result of Fe^{2+} ions inside ZnO for the Fe and Na co-dopants reported by Gu et al. [23]. The 2p peak position corresponding to 74.1 eV in Fig. 5(c) suggests the presence of Al^{3+} in ZnO, which is different from the binding energy (74.6 eV) of Al_2O_3 [15].

Fig. 5d-f represent the asymmetric O1s, oxygen peak of the undoped ZnO, ZFO: 1% Al and ZFO: 5% Al thin films. The observed peaks centered at 530.7 and 531.3 eV are ascribed to the O^{2-} (O1) and O^{2-} (O2) ions in the hexagonal wurtzite ZnO structure, attributed to the Zn-O bonding [24] and the oxygen deficient regions within the ZnO lattice or Zn-OH groups [25], respectively (Fig. 5d). The modification in O_2 peak intensity may be related to the oxygen vacancies (V_o) concentration as it decreases by enhanced Al doping contents with the constant doping level of Fe. Comparatively, it is higher in ZFO: 1% Al (Fig. 5e) than that of the ZFO: 5% Al thin films (Fig. 5d).

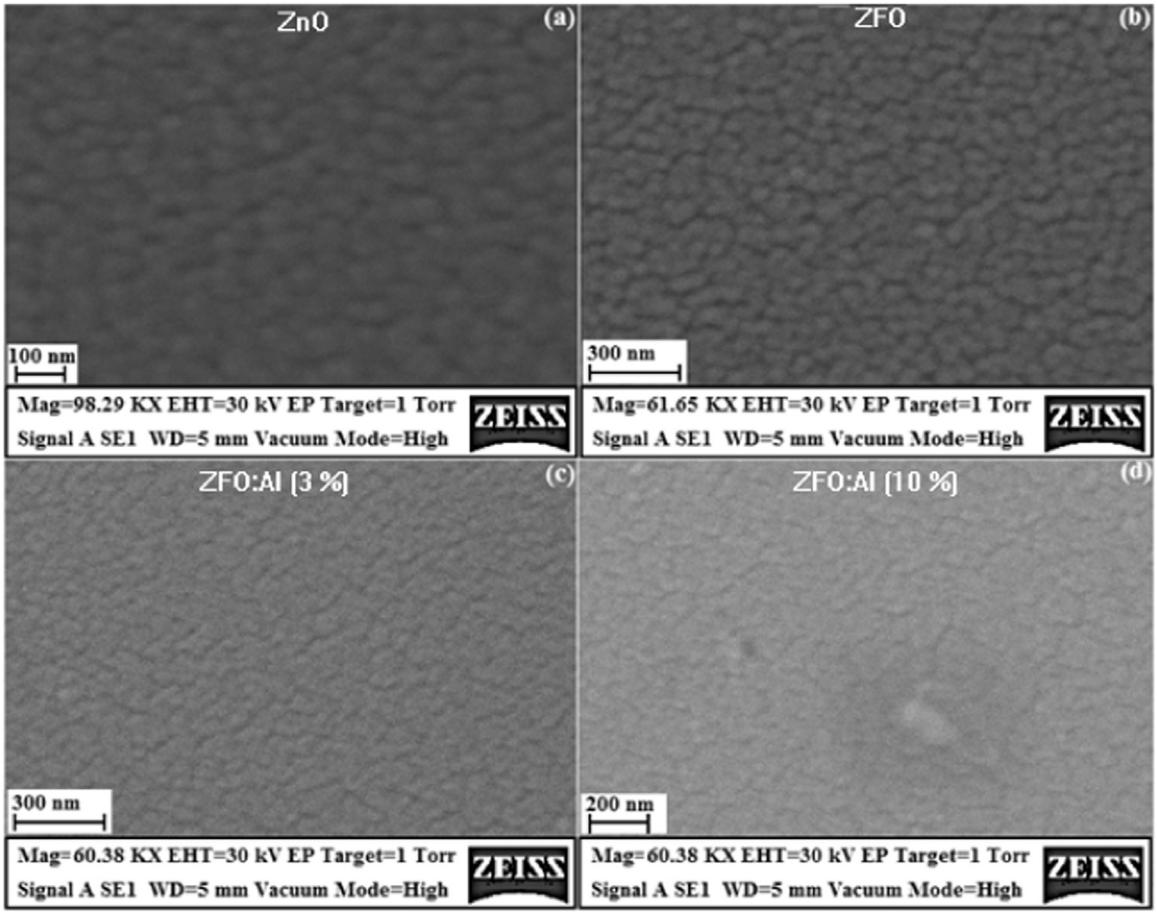

Fig. 2. SEM images of (a) ZnO, (b) ZFO, (c) ZFO: Al (3%), (d) ZFO: Al (10%) and (e-g) ZFO: Al (1%) thin films annealed at different T_A.

3.2. Optical properties

Optical transmission and absorption spectra of the Al-doped ZFO thin films were determined for the wavelengths ranging from 300 to 900 nm. The results are illustrated in Fig. 6(a-d). The sharp absorption edge in the wavelength range of 360–400 nm and the presence of interference fringes clearly indicate the high crystalline quality of the prepared films. Fig. 6(a) reveals that the transparency of the films increases in visible range via co-doping of Fe and Al. A possible reason behind this phenomenon is the decrement of disorders in the films resulting a decrease in scattering of photons. We distinctly present the inset of Fig. 6(b) to show red and the blue-shifts of absorption edge corresponding to the Fe and Al dopants, respectively.

It is known that the optical band gap (E_g) of the samples can be obtained via Tauc equation [5] using the absorption spectra. Fig. 6(c) exhibits a decrease in E_g by Fe doping while an increase in E_g by increasing Al doping ratios in comparison to the undoped ZnO films. The T_A depended E_g of 1% Al doped ZFO films represents the enhanced E_g (see Fig. 6(d) and Table 2). The reduction of E_g by Fe doping can probably be ascribed to the sp–d spin-exchange interactions between the band electrons and the localized d electrons of the transition-metal ion [3]. On the other hand, the increment of E_g via Al doping ratio and T_A resemble the Burstein–Moss effect [25] resulting from the enhanced carrier concentration comparing with undoped ZnO films. In addition, it is found that the E_g has the same trend with the *sGB* by Fe doping and Fe and Al co-doping in ZnO. However, E_g shows inversely proportional with the *sGB* by increased T_A.

The refractive index (n) of materials is one of the most important optical parameters that is inversely correlated with E_g [26] given by the equation:

$$\frac{n^2-1}{n^2+1} = 1 - \left(\frac{E_g}{20} \right)^{1/2} \quad (1)$$

The calculated values of n were summarized in Table 2. The results are in good agreement with previous studies [27,28]. We note that the n values increase by Fe doping and T_A and decrease by increasing the Al doping level as compared with pure ZnO. It is also observed that n values are inversely proportional with the *sGB* by doping of Fe and Al and increased T_A. The other important optical constant is the extinction coefficient (k), which can be calculated by using the absorption data given in Fig. 6b. We therefore used the fundamental equation below to calculate k values,

$$k = \frac{\alpha\lambda}{4\pi} \quad (2)$$

where λ is the wavelength of the incident photon and α is the absorption coefficient, which is related to the absorbance and the film thickness. The variation of k versus λ is shown in Fig. 7. We see a sharp

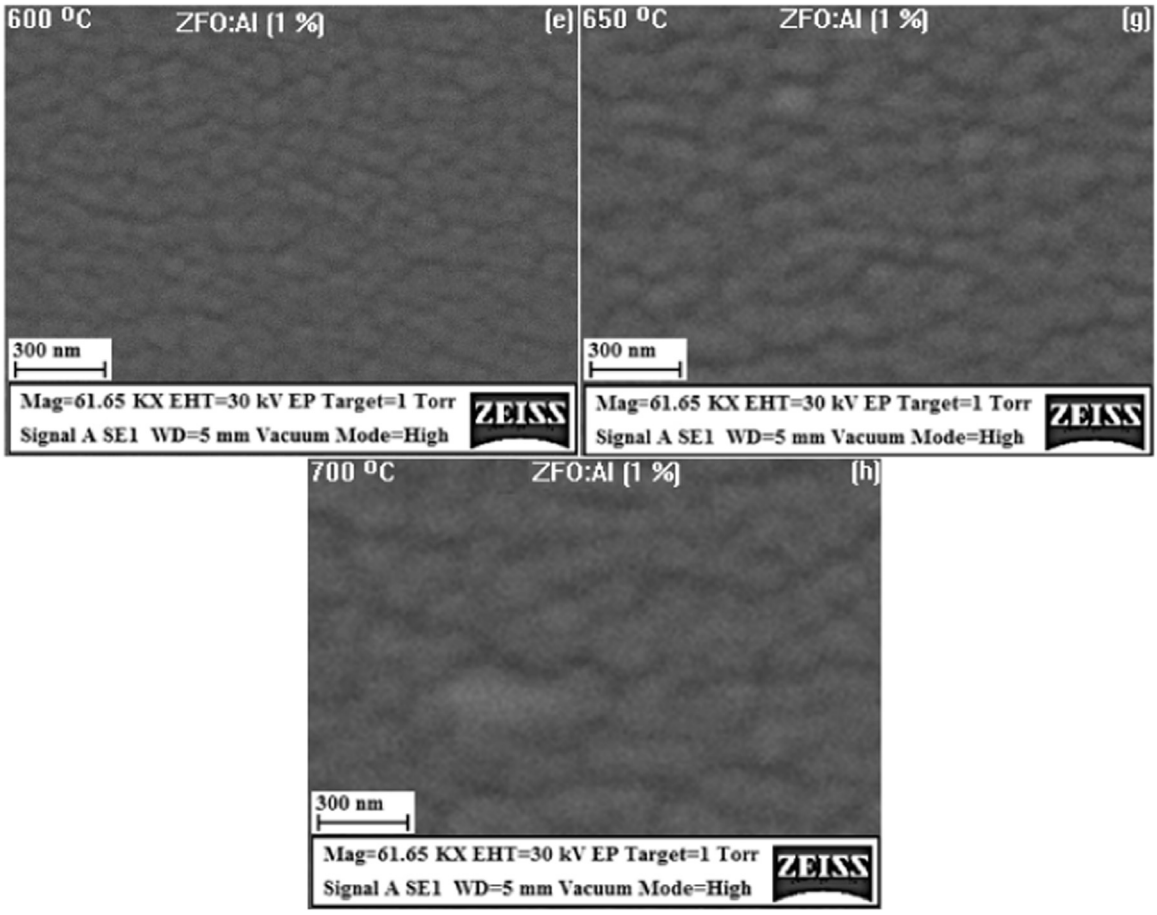

Fig. 2. (*continued*)

decrease in the wavelength range of 360–400 nm and gradual decrease within the wavelength interval of 400 and 850 nm. The k values at a wavelength corresponding to the E_g of the films are presented in Table 2. In contrast to that changes in n values are different manner via doping of Fe and higher level doping of the Al, k values regularly persist on increasing direction similar to the *sGB*. However, it decreases by T_A possibly due to the improved crystalline quality of the films and decreased *sGB*.

3.3. Electrical properties

Electrical properties such as resistivity (ρ), charge carrier concentration (n_c) and Hall mobility (μ_H) of the undoped and Al-doped ZFO thin films were obtained by Hall measurement using the van der Pauw four probe technique at room temperature. The results are summarized in Table 3. The Hall measurements clearly reveal that all the films are n-type semiconductors. It is observed that the resistivity initially increases with Fe-dopant. Then it starts to decrease at lower levels of Al doping (1%, 3%, and 5%) and suddenly increases when reaching 10% Al. This trend continues at even higher Al-doping levels. Higher values of the resistivity at Al-doping levels higher than 5% are likely attributed to the limited solubility of Al content in ZnO resulted in the formation of defects [29,30]. These defects act as carrier traps. This fact is also supported by the decrement of n_c and μ_H at these Al-doping levels, resulting from smaller grain sizes and higher *sGB* of the films.

It is useful here to mention that smaller grain sizes lead to higher grain boundary scattering. Hence, decreases in μ_H values and increases in ρ values are not surprising. It has indeed been reported by Yi et al. [31] that increasing free carrier concentration due to higher levels of Al substitution at Zn sites is a major cause of obtaining low μ_H value. The same situation has also been founded in Table 3 for the Al^{+3}-doped ZFO thin films. It is also observed that the increased T_A leads to the enhanced grain size and decreased *sGB* of the films resulting in increment and reduction of μ_H and ρ values, respectively. This is likely due to the decrease in grain boundary scattering because of the small *sGB*.

3.4. Magnetic properties

We finally examine magnetic properties of the Al-doped ZFO thin films under consideration. The magnetic field was applied parallel to the direction of films, changing from 10.000 to −10.000 Oe during the VSM measurements. The diamagnetic contribution of sample holder was accordingly subtracted from the data for all the films. The results are presented in Figs. 8a-c and 9a-b by means of the applied field dependent magnetization (M-H) and the temperature dependent magnetization (M-T) curves, respectively.

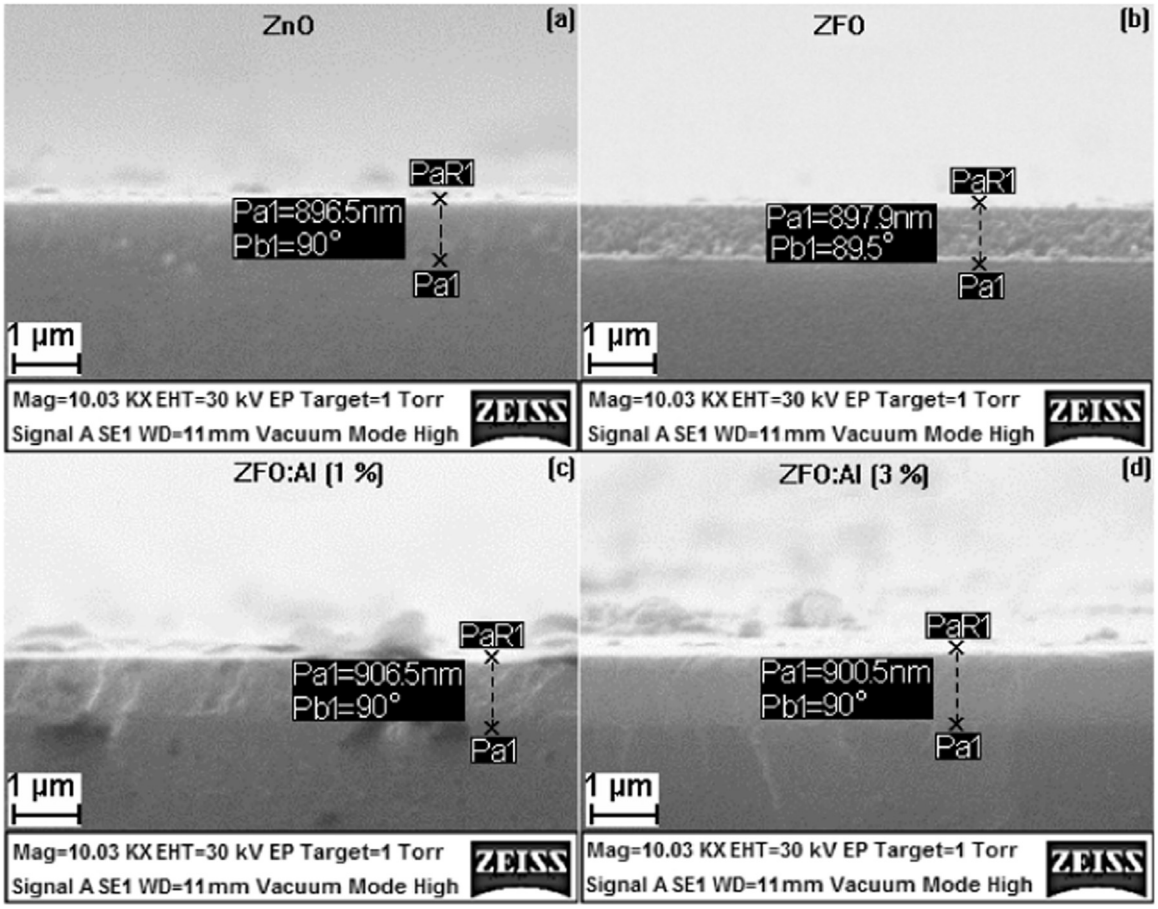

Fig. 3. SEM cross-section images of (a) ZnO, (b) ZFO, (c) ZFO: Al (1%) and (d) ZFO: Al (10%) thin films.

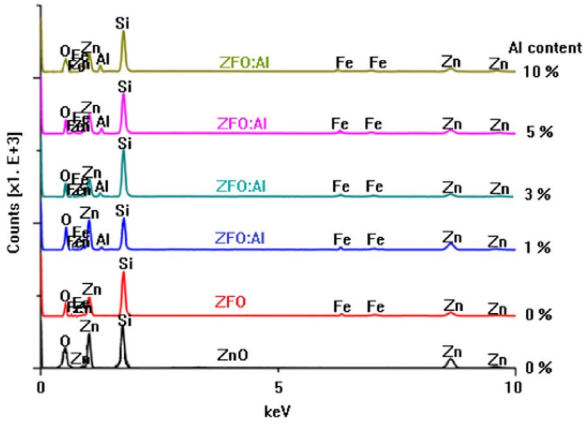

Fig. 4. EDX spectrums of ZnO, ZFO and ZFO: Al (1%, 3%, 5% and 10%) thin films.

It is seen that the ZFO film shows no ferromagnetic response, as clearly reported earlier [3]. However, all the Al-doped films show ferromagnetic response at room temperature, as similar to those given in Fig. 8(a) and (b). As the levels of Al doping are increased from 5% to 10%, the ferromagnetic responses decrease, probably due to the reduced relative distance between Al^{3+} ions and the formation of carrier traps relatively at a higher level of Al (5% and 10%), which lead to reduction of ferromagnetic interactions. The increased ferromagnetic response at different T_A (Fig. 8c) which is mainly due to the improved crystalline quality or grain size effect [32] of the 1% Al-doped ZFO samples.

The M-T curves of the undoped and Al-doped ZFO films under applied magnetic field of 500 Oe are presented in Fig. 9a-b. It was observed that the magnetization of the Al-doped ZFO films was higher than that of ZFO thin films indicating the ferromagnetic nature of the 1% and 3% Al-doped ZFO films. As seen in Fig. 9b the magnetization of the 1% Al-doped ZFO samples was enhanced by T_A. Inset of Fig. 9b clearly represents the increment of Curie temperature, T_C with enhanced T_A related to improved crystalline quality and hence grain size [33]. The magnetization of the Al-doped ZFO films was increased with reduction of temperature and no transition to ferromagnetic phase at low temperatures. Comparatively, the magnetization of the Al-doped (1% and 3%) ZFO was higher than that of Al-doped (5% and 10%) ZFO as confirmed by M-H curves. The observed S shaped curves were due to the ferromagnetism of the Al-doped ZFO films. The S shaped curves were also previously observed by Gu et al. for the ZFO nanoparticles [23].

As supported by XRD results, no secondary phases due to incorporation of Fe and Al in ZnO thin films. As seen in Fig. 9a-b, there are no ferromagnetic or anti ferromagnetic phase transition belongs to FeO, γ-Fe_2O_3, Fe_3O_4, and $ZnFe_2O_4$ secondary phases since FeO and $ZnFe_2O_4$ are antiferromagnetic with Neel temperature (T_N) of 291 and 10 K while γ-Fe_2O_3 and Fe_3O_4 are ferromagnetic with high T_C of 873

and 858 K, respectively [3]. These results highly support the possibility of ferromagnetism originated from the proper incorporation of Al and Fe dopants into the ZnO lattice site.

It is worth to explain here the observed enhanced room temperature ferromagnetism (RTFM) depending on T_A, which is one of the most important outcomes of this investigation. There are several possible causations for the RTFM in case of the Al-doped ZFO thin films. It is reported that the n-type carriers produced through Al dopant can be considered as the main determinant to cause RTFM [15]. This is known as the Ruderman Kittel Kasuya Yoshida, RKKY [34] theory, also known as carriers-mediated ferromagnetism theory that suggests incorporation of Al into ZFO system to create free carriers and ferromagnetism [35]. This drives the exchange coupling between the local spin polarized *d* orbital electron of Fe^{2+} ions mediated through free delocalized carriers of Al^{3+} [19]. It is impossible to attribute the observed RTFM to RKYY model since the used Fe and Al concentrations are small enough (few percent doping). Cao et al. [15] reported increased ferromagnetic response with increasing concentration of Al^{+3} in ZnCoO thin films. However, Al-doped ZFO thin films studied here show increased Al^{+3} doping levels as the ferromagnetic response decreases, which was not expected. This is possibly ascribed to the reduced relative distance between Al^{3+} ions for the higher level of Al doing concentrations (5% and 10%). On the other hand, Gao et al. [36] have reported that the RTFM could be due to the point defects such as Zn interstitial and V_o, which can be the main reasons for the observed RTFM. Additionally, clustering or secondary phases related to Fe is also one of the main factor to induce RTFM in Al-doped ZFO system [15,19]. In our case, however, there is no evident of clustering Fe or such phases due to the Fe doping (see XPS and XRD results presented above). Moreover, Coey et al. [37] has been suggested that the bound magnetic polaron model, which has magnetic exchange involving a spin-polarized electron trapped at an oxygen vacancy. For the present Al-doped ZFO thin films, the increased Al doping content does not lead to an increase in RTFM response. Hence, the observed RTFM cannot be attributed to the bound magnetic polaron. Furthermore, it has been suggested that RTFM can be attributed to the grain boundaries effect [22] and it is an important key parameter for TM-doped ZnO having ferromagnetic behaviour. According to the *s*GB of presented ZnO, it has non ferromagnetic behaviour as we experimentally proved. Because its *sGB* value (47.1×10^6 m^2/m^3) is lower than that of a certain critical value (s_{th}) 5.3×10^7 m^2/m^3, which is theoretically calculated [22]. For all Fe and Al co-doped ZnO samples *sGB* values are higher than s_{th} value 5×10^4 m^2/m^3 suggesting ferromagnetic behaviour according to the theory [22,38]. Among the doped samples only Fe-doped ZnO has not ferromagnetic response according to magnetic measurements. Therefore, the presented Fe-doped ZnO does not obey the theoretical calculations suggested by Straumal et al. [39]. Finally, it can be concluded that the observed RTFM in Al-doped ZFO thin films is likely due to the point defects like Zn interstitial or V_o (see Fig. 5d-f). It is known that the oxygen vacancies, increased by doping atoms (Fe, Al) can diffuse into interstitial or interstitial-granular positions without disturbing the host structure enhancing the magnetic response of the samples. Additionally, the effect of grain boundaries cannot be neglected in solution processed in Fe and Al co-doped ZnO thin films.

4. Conclusions

The role of annealing temperature, Fe and Al co-doping on the structural, optical, electrical and magnetic properties of ZnO thin films are studied in detail. The unique sol-gel derived Al-doped ZFO thin films are obtained and experimentally examined for this purpose. According to the results obtained here, the sol-gel synthesized Al-doped ZFO thin films can be identified by the following characteristics: (1) The polycrystalline nature of the films and a single hexagonal wurtzite phase belonging to ZnO with a preferred orientation along the c-axis of hexagonal wurtzite structure; (2) the crystallization of the films has deteriorated on Fe doping and increased by Al doping ratio as well as T_A; (3) a homogeneous distribution of the grains on the film surfaces and a decrement or increment of the grain size through Fe and Al

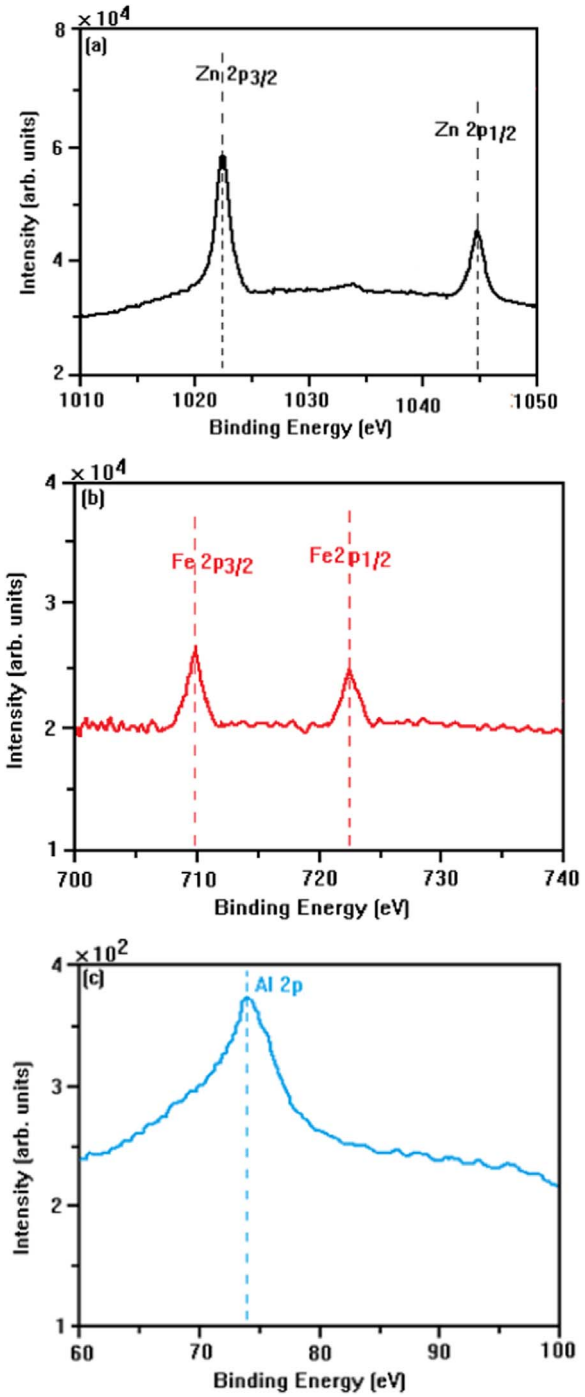

Fig. 5. (a) Zn, (b) Fe and (c) Al 2p XPS spectra of ZFO: Al (3%) thin films and O1s XPS spectra of ZnO (d), ZFO: Al (1%) (e) and ZFO: Al (5%) (f) thin films.

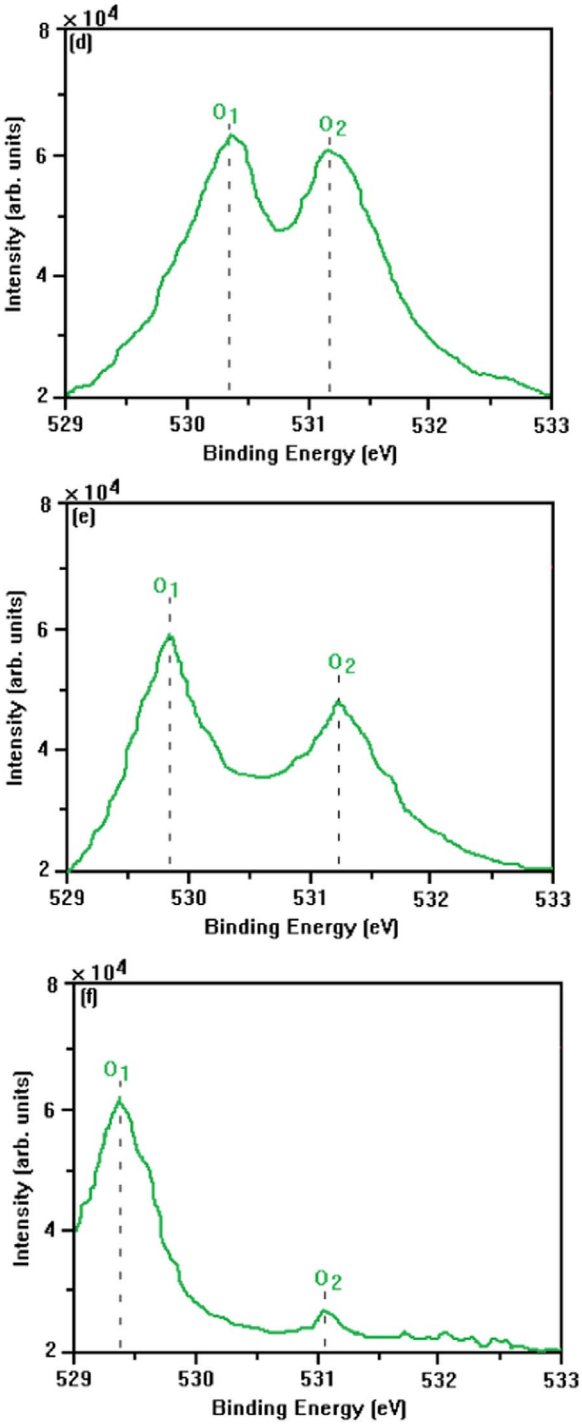

Fig. 5. (*continued*)

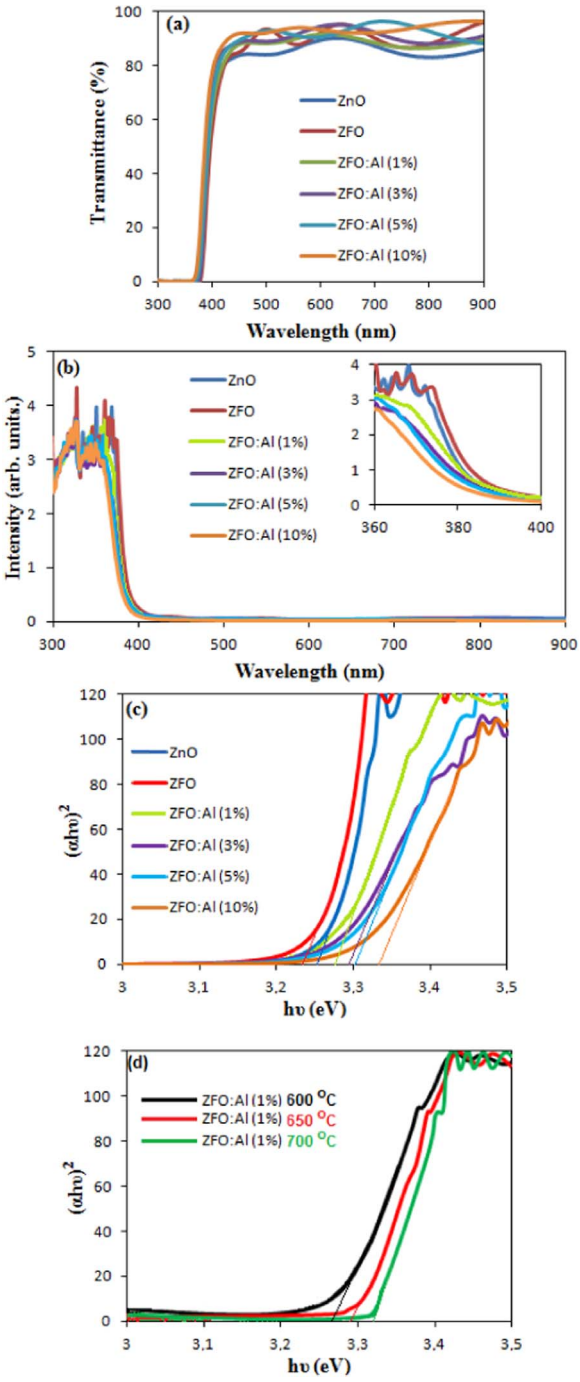

Fig. 6. Optical (a) transmission, (b) absorption (inset: wide-scan absorption spectra between 360 and 400 nm) spectrums and (c) the plots of $(\alpha h\upsilon)^2$ vs. photon energy for the ZnO, ZFO, ZFO: Al (1%, 3%, 5% and 10%) and (d) T_A depended ZFO: Al (1%) thin films.

doping and T_A, respectively; (4) the films have presence of Zn^{2+}, Al^{3+} and Fe^{2+} ions; (5) a clear decrement and increment of the optical band gap from 3.25 to 3.23 eV and from 3.23 to 3.34 eV for the Fe and Al dopants, respectively; (6) an increase in the optical band gap by T_A is also found; (7) compared with ZnO the refractive index of the films first increases and then decreases while the extinction coefficient increases with doping of Fe and Al, at wavelength corresponding to band gap energy, respectively; (8) the enhanced T_A results in a decrement of the extinction coefficient while the increment of refractive index for the 1% Al-doped ZFO films; (9) the films have n-type conductivity and the

Table 2
Variation of selected optical characteristics as a function of Fe and Al dopants in ZnO thin films depended on T_A.

Chemical composition	E_g (eV)	n	k	T_A(°C)
ZnO	3.25	1.992	0.029	600
ZFO	3.23	2.004	0.030	600
ZFO: Al (1%)	3.28	1.973	0.035	600
ZFO: Al (3%)	3.29	1.968	0.038	600
ZFO: Al (5%)	3.31	1.956	0.042	600
ZFO: Al (10%)	3.34	1.938	0.045	600
ZFO: Al (1%)	3.29	1.968	0.032	650
ZFO: Al (1%)	3.32	1.975	0.028	700

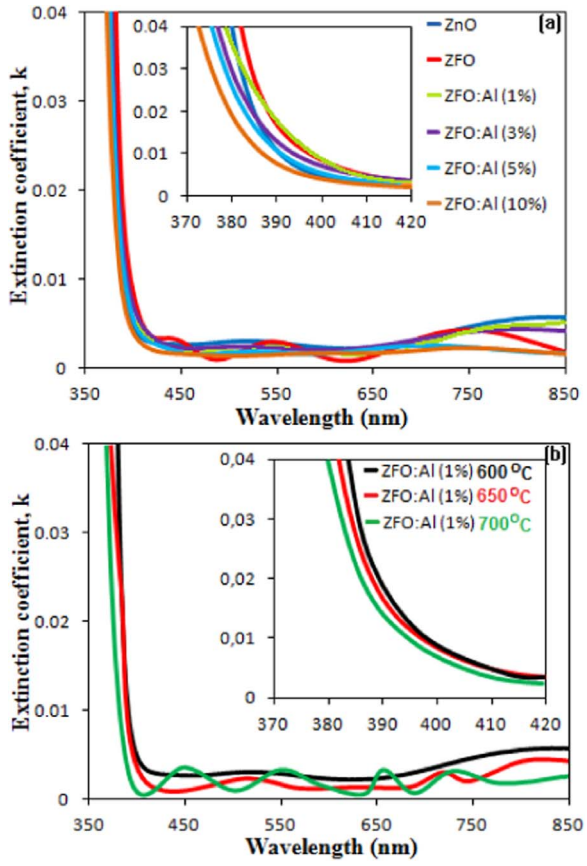

Fig. 7. Variation of extinction coefficient as function of wavelength for the for the (a) ZnO, ZFO, ZFO: Al (1%, 3%, 5% and 10%) and (b) T_A depended ZFO:Al (1%) thin films.

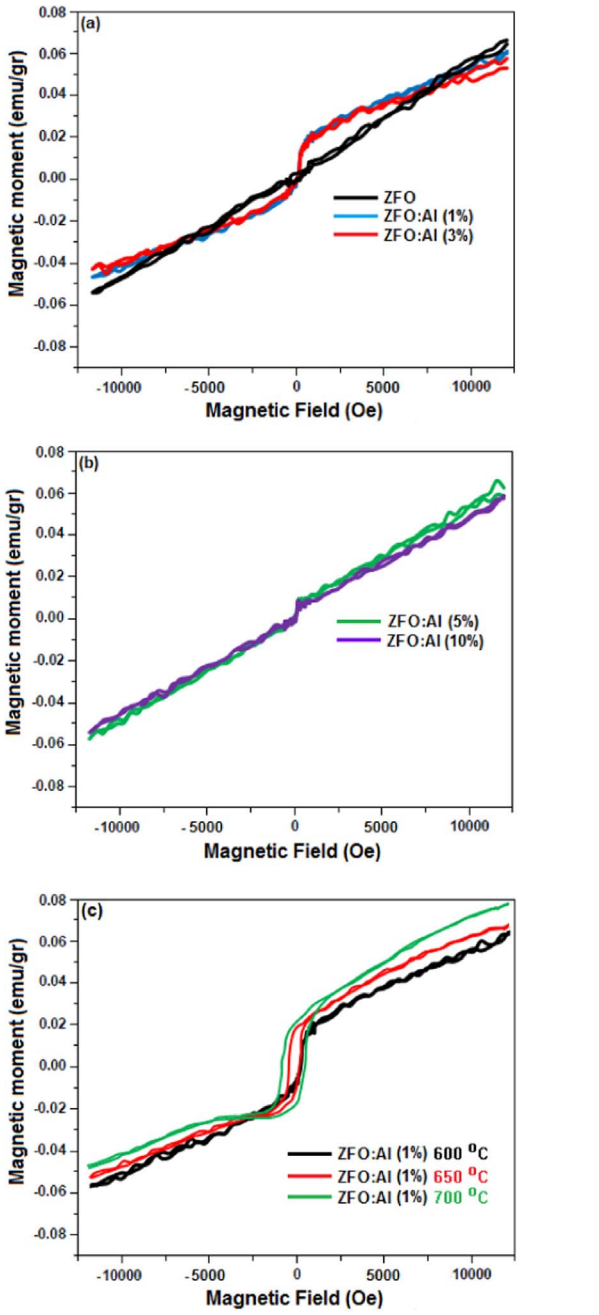

Fig. 8. Room temperature M-H curves for the (a) ZFO and ZFO: Al (1% and 3%), (b) ZFO: Al (5% and 10%) and (c) T_A depended ZFO: Al (1%) thin films.

enhancement of the charge carrier concentration with raising Al-doping concentration and T_A; (10) the oxygen-vacancies and grain boundaries induce RTFM in Al and Fe doped ZnO thin films; and (11) the enhanced RTFM by T_A in 1% Al-doped ZFO thin films.

The results obtained here are in well agreement with previous reports, in terms of physical mechanism behind the T_A induced physical properties of ZnO, doped with various transition metals. However, this study is the first to report sol-gel synthesized Al-doped ZFO thin films and the results impressively suggest that such thin films are potentially attractive candidates for spintronic and optoelectronic applications.

Table 3
Electrical parameters of the ZnO, ZFO and ZFO: Al (1%, 3%, 5% and 10%) thin films depended on T_A.

Chemical composition	Cariers concentration (n_c) (cm^{-3})	Resistivity (ρ) (Ω cm)	Mobility (μ) (cm^2/Vs)	Cariers type	T_A (°C)
ZnO	4.66×10^{14}	2.56×10^{3}	5.24×10^{0}	n	600
ZFO	5.12×10^{10}	1.89×10^{5}	6.45×10^{2}	n	600
ZFO: Al (1%)	4.29×10^{13}	3.01×10^{3}	4.84×10^{1}	n	600
ZFO: Al (3%)	4.70×10^{14}	8.55×10^{2}	1.55×10^{1}	n	600
ZFO: Al (5%)	1.18×10^{15}	7.32×10^{2}	7.23×10^{0}	n	600
ZFO: Al (10%)	1.24×10^{15}	1.11×10^{3}	4.53×10^{0}	n	600
ZFO: Al (1%)	4.85×10^{13}	2.66×10^{3}	5.47×10^{1}	n	650
ZFO: Al (1%)	5.42×10^{13}	2.38×10^{3}	6.11×10^{1}	n	700

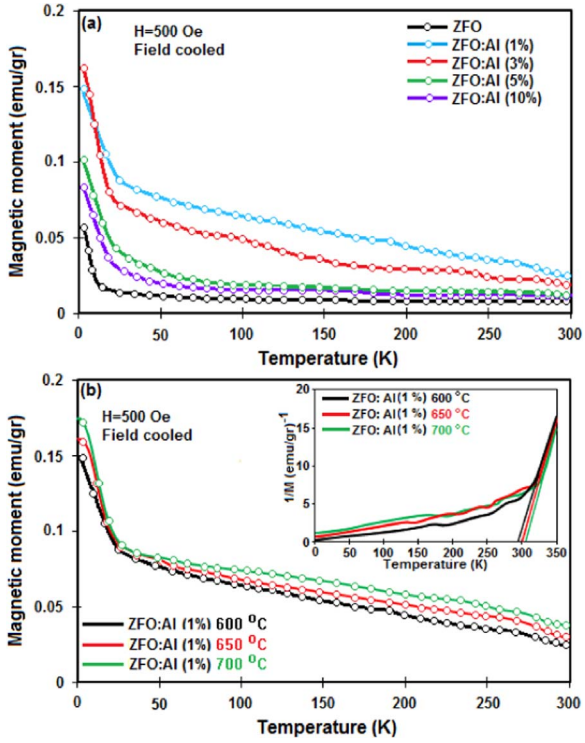

Fig. 9. M-T curves for the Fe-doped ZnO, ZFO: Al (1%, 3%, 5%, and 10%) and (b) T_A depended ZFO: Al (1%) thin films (Inset: temperature depended 1/M for T_A depended ZFO: Al (1%) thin films).

Acknowledgements

Financial supports by the Scientific Research Project Commission of Harran University (HUBAK) under Projects No. 15091, Y15018 and by the Ministry of Development of Turkish Republic under Project No. 2011K/120300 are gratefully acknowledged.

References

[1] A. Goktas, I.H. Mutlu, Y. Yamada, E. Celik, Influence of pH on the structural optical and magnetic properties of $Zn_{1-x}Mn_xO$ thin films grown by sol–gel method, J. Alloy. Compd. 553 (2013) 259–266.
[2] S.S. Nkosi, I. Kortidis, D.E. Motaung, G.F. Malgas, J. Keartland, E. Sideras-Haddad, A. Forbes, B.W. Mwakikungac, S. Sinha-Ray, G. Kiriakidis, Orientation-dependent low field magnetic anomalies and room-temperature spintronic material – Mn doped ZnO films by aerosol spray pyrolysis, J. Alloy. Compd. 579 (2013) 485–494.
[3] A. Goktas, I.H. Mutlu, Y. Yamada, Influence of Fe-doping on the structural, optical, and magnetic properties of ZnO thin films prepared by sol–gel method, Microstr. 57 (2013) 139–149.
[4] F.L. Xian, L.H. Xu, X.X. Wang, X.Y. Li, Crystallographic, optical and magnetic properties of Co-doped ZnO thin films synthesized by sol gel route, Cryst. Res. Technol. 47 (2012) 423–428.
[5] A. Goktas, F. Aslan, A. Tumbul, S.H. Gunduz, Tuning of structural, optical and dielectric constants by various transition metal doping in ZnO:TM (TM = Mn, Co, Fe) nanostructured thin films: A comparative study, Ceram. Int. 43 (2017) 704–713.
[6] T. Dietl, H. Ohno, F. Matsukura, J. Cibert, D. Ferrand, Zener model description of ferromagnetism in zinc-blende magnetic semiconductors, Science 287 (2000) 1019–1022.
[7] S.M. Chou, L.G. Teoh, W.H. Lai, Y.H. Su, M.H. Hon, ZnO: Al thin film gas sensor for detection of ethanol vapor, Sensors 6 (2006) 1420–1427.
[8] J.X. Wang, X.W. Sun, Y. Yang, C.M.L. Wu, N-P transition sensing behaviors of ZnO nanotubes exposed to NO2 gas, Nanotechnology 20 (2009) 465501–465504.
[9] D. Sridevi, K.V. Rajendran, Synthesis and optical characteristics of ZnO nanocrystals, Bull. Mater. Sci. 32 (2009) 165–168.
[10] J. Lee, D. Lee, D. Lim, K. Yang, Structural, electrical and optical properties of ZnO:Al films deposited on flexible organic substrates for solar cell applications, Thin Solid Films 515 (2007) 6094–6098.
[11] D.C. Kundaliya, S.B. Ogale, S.E. Lofland, S. Dhar, C.J. Metting, S.R. Shinde, On the origin of high-temperature ferromagnetism in the low-temperature-processed Mn–Zn–O system, Nat. Mater. 3 (2004) 709–714.
[12] C.J. Cong, J.H. Hong, K.L. Zhang, Effect of atmosphere on the magnetic properties of the Co doped ZnO magnetic semiconductors, Mater. Chem. Phys. 113 (2009) 435–440.
[13] F. Wang, W.-W. Huang, S.-Y. Li, A.-Q. Lian, X.-T. Zhang, W. Cao, The magnetic properties of $Fe_xZn_{1-x}O$ synthesized via the solid-state reaction route: Experiment and theory, J. Magn. Magn. Mater. 340 (2013) 5–9.
[14] Z.L. Lu, W. Miao, W.Q. Zou, M.X. Xu, F.M. Zhang, Enhanced ferromagnetism in single crystalline Co-doped ZnO thin films by Al codoping, J. Alloys Compd. 494 (2010) 392–395.
[15] P. Cao, Y. Bai, D.X. Zhao, D.Z. Shen, The effect of Al^{3+} co-doping on the structural, magnetic and optical properties of ZnCoO thin films, Mater. Sci. Semicon. Proc. 14 (2011) 73–77.
[16] M. Saleem, S.A. Siddiqi, Shahid Atiq, M.S. Anwar, I. Hussain, S. Alam, Carriers-mediated ferromagnetic enhancement in Al-doped ZnMnO dilute magnetic semiconductors, Mater. Charact. 62 (2011) 1102–1107.
[17] T. Thangeeswari, M. Priya, J. Velmurugan, Enhancement in the optical and magnetic properties of ZnO: Co implanted by Gd^{3+} nanoparticles, J. Mater. Sci: Mater. Electr 26 (2015) 2436–2444.
[18] M. Ashokkumar, S. Muthukumaran, $Zn_{0.91}Cu_{0.04}M_{0.05}O$ (M = Ni, Co, Cr) nanocrystals: Structural study and energy gap tailoring, Mater. Lett. 131 (2014) 302–305.
[19] S. Chattopadhyay, T.K. Nath, A.J. Behan, J.R. Neal, D. Score, Q. Feng, G.A. Gehring, Enhancement of room temperature ferromagnetism of Fe-doped ZnO epitaxial thin films with Al co-doping, J. Magn. Magn. Mater. 323 (2011) 1033–1039.
[20] M. Saleem, M.S. Anwar, A. Mahmood, S. Atiq, S.M. Ramay, S.A. Siddiqi, Defects induced magnetization in B-doped ZnFeO dilute magnetic semiconductor, Pyhsica B 465 (2015) 16–20.
[21] T.C. Kaspar, T. Droubay, S.M. Heald, P. Nachimuthu, C.M. Wang, V. Shutthanandan, C.A. Johnson, D.R. Gamelin, S.A. Chambers, Lack of ferromagnetism in n-type cobalt-doped ZnO epitaxial thin films, New J. Phys. 10 (2008) 055010–055018.
[22] Boris B. Straumal, Svetlana G. Protasova, Andrei A. Mazilkin, Eberhard Goering, Gisela Schütz, Petr B. Straumal, Brigitte Baretzky, Ferromagnetic behaviour of ZnO: the role of grain boundaries, J. 7 (2016) 1936–1947.
[23] Hao Gu, Yinzhu Jiang, Mi Yan, Defect-induced room temperature ferromagnetism in Fe and Na co-doped ZnO nanoparticles, J. Alloy. Compd. 521 (2012) 90–94.
[24] V. Kumar, F. Singh, O.M. Ntwaeaborwa, H.C. Swart, Effect of Br^{+6} ions on the structural, morphological and luminescent properties of ZnO/Si thin films, Appl. Surf. Sci. 279 (2013) 472–478.
[25] E. Burstein, Anomalous optical absorption limit in InSb, Phys. Rev. 93 (1954) 632–633.
[26] P.T. Hsieh, Y.C. Chen, K.S. Kao, C.M. Wang, Luminescence mechanism of ZnO thin film investigated by XPS measurement, Appl. Phys. A 90 (2008) 317–321.
[27] J. Bian, X. Li, L. Chen, Q. Yao, Properties of undoped n-type ZnO film and N–In codoped p-type ZnO film deposited by ultrasonic spray pyrolysis, Chem. Phys. Lett. 393 (2004) 256–259.
[28] J.S. Wellings, N.B. Chaure, S.N. Heavens, I.M. Dharmadasa, Growth and characterisation of electrodeposited ZnO thin films, Thin Solid Films 516 (2008) 3893–3898.
[29] H. Benzarouk, A. Drici, M. Mekhnache, A. Amara, M. Guerioune, J.C. Bernede, H. Bendjffal, Effect of different dopant elements (Al, Mg and Ni) on microstructural, optical and electrochemical properties of ZnO thin films deposited by spray pyrolysis (SP), Microstr. 52 (2012) 594–604.
[30] J. Hu, R.G. Gordon, Textured aluminum-doped zinc oxide thin films from atmospheric pressure chemical-vapor deposition, J. Appl. Phys. 71 (1992) 880–890.
[31] A.F. Aktaruzzaman, G.L. Sharma, L.K. Malhotra, Electrical, Optical and annealing characteristics of ZnO:Al films prepared by spray pyrolysis, Thin Solid Films 198 (1991) 67–74.
[32] A. Göktaş, A. Tumbul, F. Aslan, Grain size-induced structural, magnetic and magnetoresistance properties of $Nd_{0.67}Ca_{0.33}MnO_3$ nanocrystalline thin films, J. Sol-Gel. Scien. Technol. 78 (2016) 262–269.
[33] A. Göktaş, İ.H. Mutlu, A. Kawashi, Growth and characterization of $La_{1-x}A_xMnO_3$ (A = Ag and K, x = 0.33) epitaxial and polycrystalline manganite thin films derived by sol–gel dip-coating technique, Thin Solid Films 520 (2012) 6138–6144.
[34] Kuo Shou-Yi, Chen Wei-Chun, Lai Fang-I, Cheng Chin-Pao, Kuo Hao-Chung, Wang Shing-Chung, Effects of doping concentration and annealing temperature on properties of highly-oriented Al-doped ZnO films, J. Cryst. Growth 287 (2006) 78–84.
[35] D.J. Priour Jr, E.H. Hwang, S.D. Sarma, Disordered RKKY lattice mean field theory for ferromagnetism in diluted magnetic semiconductors, Phys. Rev. Lett. 92 (2004) 117201–117204.
[36] D.Q. Gao, D.S. Xue, Y. Xu, Z.J. Yan, Z.H. Zhang, Synthesis and magnetic properties of Cu-doped ZnO nanowire arrays, Electrochim. Acta 54 (2009) 2392–2395.
[37] J.M.D. Coey, A. Douvalis, C. Fitzgerald, M. Venkatesan, Ferromagnetism in Fe-doped SnO_2 thin films, Appl. Phys. Lett. 84 (2004) 1332–1335.
[38] B.B. Straumal1, A.A. Mazilkin, S.G. Protasova, S.V. Stakhanova, P.B. Straumal, M.F. Bulatov, Th Tietze, E. Goering, B. Baretzky, Grain boundaries as a source of ferromagnetism and increased solubility of Ni in nanograined ZnO, Rev. Adv. Mater. Sci. 41 (2015) 61–71.
[39] B.B. Straumal, S.G. Protasova, A.A. Mazilkin, P.B. Straumal, G. Schütz, Th Tietze, E. Goering, B. Baretzky, Ferromagnetic behaviour of Fe-doped ZnO nanograined films, Beilstein J. Nanotechnol 4 (2013) 361–369.